



# Selenium Mitigates Ammonia-Induced Neurotoxicity by Suppressing Apoptosis, Immune Imbalance, and Gut Microbiota-Driven Metabolic Disturbance in Fattening Pigs

Yutao Li<sup>1,2</sup> · Jing Wang<sup>2</sup> · Houjuan Xing<sup>3,4</sup> · Jun Bao<sup>2,4</sup>

Received: 29 June 2022 / Accepted: 24 September 2022

© The Author(s), under exclusive licence to Springer Science+Business Media, LLC, part of Springer Nature 2022

## Abstract

Ammonia could be regarded as one detrimental pollutant with an acrid smell in livestock sheds. So far, the pig breeding industry became the main source of atmospheric ammonia. Previous literature demonstrated that excessive ammonia inhalation might cause a series of physiological damage to multiple organs. Unfortunately, the toxicity mechanisms of gaseous ammonia to the porcine nervous system need further research to elucidate. Selenium (Se) involves in many essential physiological processes and has a mitigative effect on the exogenous toxicant. There were scant references that corroborated whether organic Se could intervene in the underlying toxicity of ammonia to the hypothalamus. In the present study, multi-omics tools, ethology, and molecular biological techniques were performed to clarify the detailed mechanisms of relaxation effects of L-selenomethionine on ammonia poisoning. Our results showed that ammonia inhalation caused the clinical symptoms and the increment of positive apoptosis rate in the hypothalamus with the dysfunction of mitochondrial dynamics factors, while obvious mitochondria structure defects were observed. In parallel, the inflammation medium levels and gut microbes-driven metabolism function were altered to mediate the neurotoxicity in fattening pigs through the initiation of inflammation development. Interestingly, L-selenomethionine could attenuate ammonia toxicity by activating the PI3K/Akt/PPAR- $\gamma$  pathway to inhibit the mitochondria-mediated apoptosis process, blocking the abnormal immune response and the accumulation of reactive oxygen species in the nucleus. Meanwhile, Se could enhance the production performance of fattening sows. Taken together, our study verified the novel hypothesis for the toxicity identification of aerial ammonia and provided a therapeutic strategy for the treatment of occupational poisoning.

**Keywords** Ammonia · Neurotoxicity · Apoptosis · Selenium · PI3K/Akt/PPAR- $\gamma$  axis · Pig

## Introduction

With the rapid development of the intensive production model in animal husbandry, animal welfare has been brought to more attention. Intensive agriculture led to the accumulation of excrement and feed residue in livestock houses [1]. Under the decomposition roles of microbiota, these substances could generate a series of harmful gases with foul odors. Ammonia, a major alkaline gas with a pungent smell in the atmosphere [2], could dissolve in water in arbitrary proportion [3]. Based on existing references, environmental pollutants generated by industrialized pig farms usually took the dominant position in animal production, while ammonia was regarded as the primary toxic substance in piggeries [4]. With the gradual expansion of agricultural intensification, husbandry production has become an important source of gaseous ammonia emission [5]. Thereinto, pig

✉ Houjuan Xing  
xinghoujuan@neau.edu.cn

✉ Jun Bao  
jbao@neau.edu.cn

<sup>1</sup> College of Life Science, Northeast Normal University, Changchun 130117, People's Republic of China

<sup>2</sup> College of Life Science, Northeast Agricultural University, Harbin 150030, People's Republic of China

<sup>3</sup> College of Animal Science and Technology, Northeast Agricultural University, Harbin 150030, People's Republic of China

<sup>4</sup> Key Laboratory of Swine Facilities Engineering, Ministry of Agriculture and Rural Affairs, Harbin 150030, People's Republic of China

breeding almost accounted for 15% of ammonia emissions from global husbandry [6, 7]. Due to the imbalance between ventilation and artificial heating, ammonia accumulation has been a typical production problem. In the most enclosed pig farm, the ammonia concentration could reach  $35 \mu\text{g}\cdot\text{L}^{-1}$  throughout the year, even more than  $150 \mu\text{g}\cdot\text{L}^{-1}$  sometimes.

Except for the ecology threat [8], some reports have demonstrated that ammonia inhalation would pose physiological stress to mammals. Chronic ammonia exposure stimulated the sensory organs to decrease production performance (meat quality and average daily gain). Ammonia inhalation also led to a series of pathological symptoms in farm animals [9, 10]. After ammonia poisoning, pigs exhibited more cough frequency and aggressive behaviors. As one neurotoxin, ammonia has toxic effects on neurons, which are the potential targets of ammonia toxicity [11].

Inflammation, which benefits the tissue injury repairing of the immune system, is regarded as the programmed defense response of an organism to exogenous stimulation. Inflammation response could be induced by many inflammatory mediums (such as cytokines) [12] and was usually accompanied by pathological changes. Cytokines, which could combine with specific membrane receptors through paracrine signals, were divided into helper T cell (Th) 1 and Th2 cytokines. Th1 cytokines usually participate in cellular immunity while Th2 cytokines are related to the humoral immune [13]. Di-2-ethylhexylphosphate would induce the imbalance of Th1/Th2-related genes in neutrophils to inhibit the ability to uptake phagocytes [14]. Shi et al. also found that excessive ammonia could up-regulate the expression of Th2 cytokines (interleukin (IL)-6 and IL-10) in the trachea and down-regulate the mRNA level of interferon (IFN)- $\gamma$  (one of Th1 cytokines), accompanied by obvious inflammatory cell infiltration in trachea connective tissue [15]. Nitric oxide (NO), which was synthesized by inducible nitric oxide synthase (iNOS) [16], is also involved in the regulatory process of inflammation response. As a signaling molecule, NO also could react with pro-apoptosis factors to activate the programmed cell apoptosis process [17]. An et al. confirmed that chronic ammonia poisoning elevated the NO and iNOS levels and promoted the aggregation of leukomonocyte in the splenic cord [18, 19]. Nowadays, it has been found that dynamic gut microbes played essential roles in immunity development and pathogen invasion defense [20, 21]. As the biggest micro-ecosystem in organisms, the biological function of intestinal microorganisms could be influenced by environmental pollutants [22]. Gut microbiota are distributed on the surface of intestinal mucosa to constitute the intestinal immune barrier [23, 24]. Ren et al. reported that the microbiota diversity in the feces of coronavirus disease-2019 patients was decreased while the immunoglobulin- $\gamma$  (IgG) level in serum was elevated [25]. Specific microbial molecules stimulated the activation of

natural killer T cells and signaling transduction, participating in intestinal inflammation response and immune regulation to cause behavioral abnormalities and nervous system imbalance [26, 27].

Apoptosis is regarded as the normal physiological process to finish the cell survival cycle and remove the damaged cells in the organism's development [28]. It is thought that cell apoptosis was related to immune response, but not induced inflammatory injury directly [29]. The mitochondrial apoptosis pathway is one of the most typical apoptosis signaling pathways. Many environmental pollutants could recruit excessive reactive oxygen species (ROS) and accelerate the synthesis of cytokines to initiate the mitochondrial apoptosis pathway [30], leading to the activation of the Caspase family and the occurrence of cell apoptosis [31]. High ammonia exposure could mediate the apoptosis process in the kidney, liver, and brain [32] through altering the expression level of immune-related genes and promoting ROS accumulation in the respiratory chain [33].

Selenium (Se) is an essential trace element in the internal environment of organisms [34], and plays important roles in antioxidant defense [35] and detoxification metabolism [36]. Previous studies have demonstrated that Se had mitigative effects on the toxicity of heavy metals. Zhang et al. found that sodium selenite could decrease the inflammatory factors in the livers of the laying hens and attenuate tissue injury after cadmium exposure [37]. Oxygen radical activated the release of inflammation medium while Se could block the ROS accumulation [38]. Organic Se could modulate the oxidative stress level and inhibit the NO production to relieve the inflammation injury induced by aluminum [39]. Previous reports corroborated that Se supplement inhibited lipid peroxidation to enhance the immune defense ability. Taken together, in our study, morphology, molecular biology techniques and multiple omics were used to analyze the underlying toxicology mechanisms of ammonia and the protective roles of Se on the nervous system. Our present study would provide the theoretical basis for the veterinary medicine research.

## Materials and Methods

### Establishment of Animal Poisoning Model

Twenty-four female fattening pigs (125-day-old) with similar weight ( $48.0775 \pm 0.9292 \text{ kg}$ ) were divided into four groups, namely control group (C), Se group (Se), ammonia group (A), and ammonia + Se group (A + Se), respectively. Ammonia concentration in C and Se kept below  $5 \text{ mg}\cdot\text{m}^{-3}$ , while the ammonia concentration in another two groups was  $90.85 \pm 1.65 \text{ mg}\cdot\text{m}^{-3}$ . Meanwhile, the experimental animals in C and A group were fed with normal fodder used for fattening pigs (Se concentration was kept at  $0.33 \text{ mg}$  per kg of

diet), and the animals in Se and A + Se group were fed with a commercial diet supplemented with L-selenomethionine and Se concentration in fodder was at  $0.50 \text{ mg}\cdot\text{kg}^{-1}$  level. Detailed compositions of basal diets (W5452A, WELLHOPE, China) were shown in Table S1. All animals had free access to water and feed. In the period of the experiment, exogenous ammonia was provided by the liquid ammonia tank and controlled by the ammonia flow rate monitor automatically. Atmospheric ammonia level was monitored by an Ammonia Meter/Data Logger Model ZDL-800 (Florida, USA). During the breeding period, all environmental conditions were in line with the requirement for animal welfare (DIRECTIVE 2010–63-EU). The experiment was last for 35 days (including 5 days for acclimation of the test room). At the end of the experiment, all pigs were injected with 20% ethyl carbamate ( $1000 \text{ mg}\cdot\text{kg}^{-1}$ ) to euthanize and the hypothalamus tissue and skeletal muscle were separated on the ice box. Based on the previous research result of our lab [32], the porcine ammonia-poisoning model was established successfully.

### Measurement of Se Content in Tissue

A total of 1000 mg fresh tissue was dissolved with 30% hydrogen peroxide solution and 65% nitric acid. The mixture was digested in the microwave systems as followed: 1800 W at  $100^\circ\text{C}$  for 3 min, 1800 W at  $150^\circ\text{C}$  for 10 min, and 1800 W at  $180^\circ\text{C}$  for 45 min. In our experiment, the blank zero setting group was performed using the same method. Finally, the Se content in samples was measured using the inductively coupled plasma mass spectrometry (ICP-MS) (No. 7800, AGILENT, America). All measure procedures above were based on the internal standard method. The concentration of the standard solution was used as the abscissa and the ratio of sample signal to internal standard signal as ordinate, and the slope was obtained by linear regression method to obtain the standard curve. The relative Se content in tissue was calculated based on respective signal intensity ratios.

### Measurement of Growth Performance and Meat Quality

At the beginning of the present experiment, all sows were weighed (WO) using an electronic platform scale without taking a diet. When the pigs were anesthetized, the final weight (WS) was recorded in the same way. During the period of the whole experiment, the daily feed intake (FI) was also recorded based on the diet consumption per pig. In addition, the average daily gain (ADG) and feed conversion ratio (FC) were calculated.  $\text{ADG} = (\text{WS} - \text{WO}) / 30$ ;  $\text{FC} = \text{FI} / \text{ADG}$ .

The skeletal muscle was used to evaluate the effect of ammonia on meat quality within 50 min. A portable pH meter (HI9025C, HANNA, Italy) was used to detect the pH value. All procedure corresponded to the instruction provided by

the manufacturer. Each sample was measured three times in a random position. Fresh skeletal muscle was cut into cubes to measure the meat colour (lightness ( $L^*$ ), redness ( $a^*$ ), yellowness ( $b^*$ )) by automatic colorimeter (SMY-2000SF, Meiyu, Shanghai) according to the instruction. Shear force (SH) could be regarded as a typical indicator to evaluate the tenderness. The fresh meat in triplicate was heated by water bath until the central temperature reached  $71^\circ\text{C}$  and then cut into  $3.5 \text{ cm}^2$  strips along the fiber direction. Finally, the tenderness meter (M10, BULADER, Beijing) was used to determine the shear force. The skeletal muscle was sealed with sterile valve bags and stored at  $4^\circ\text{C}$  overnight. It's worth noting that the valve bags could not wrap the meat tightly. The initial weight was recorded (WI), and the final weight (WF) was measured after the meat sample was dried with a clear filter paper. The drip loss efficiency (DS) was calculated as followed:  $\eta = (\text{WI} - \text{WF}) / \text{WI} \times 100\%$ .

### Observation of Pathological Symptom

The feeding desire and activity degree of experimental animals were evaluated. High-definition infrared cameras were fixed to the roof of the environmental control module to cover the whole viewing angle of the colony house. The video recording sessions were set for the periods of 8:00–10:00, 12:00–14:00, and 18:00–20:00. The definition of picture quality was selected as 300 dpi and other parameters depending on the default setting. Feeding desire was expressed by the frequency of foraging behavior (the food was obtained from the tank and swallowed) during the video capture time. Activity degree was measured using the times that the animals touched (e.g. pushed, rubbed, or bit) the balls tied to the pens during the video recording period. All subjected pigs were observed and their behaviour was recorded based on the all-occurrence recording method.

### High-Throughput Reference Genome-Based Transcriptome Analysis

Total RNA was extracted using TRIzol reagent and purified with a commercial kit (DP412, TIANGEN, Beijing) to obtain a high-quality mRNA product (RNA integrity number  $> 7.0$ ). Magnetic beads with Oligo (dT) were used to enrich specific mRNA which was cut into short fragments. Six-base random primers were added to synthesize complementary DNA and two ends of the double-stranded DNA were attached with an "A" base. Finally, the sequencing library with  $300 \pm 50$  bp-length fragment was composed and paired-end sequencing was conducted using Illumina Novaseq™ 6000 sequencer [32]. Raw sequence files were deposited in the Sequence Read Archive (SRA) database of the National Center Biotechnology Information Database (Accession No. PRJNA741846). After the unqualified sequence was filtered, clean reads

were mapped into the reference genome (*Sus scrofa*) with the HISAT2-2.0.4 software. DESeq2 was used to identify the differentially expressed gene (fold change > 2.82 and  $P$  value < 0.05). Kyoto Encyclopedia of Genes and Genomes (KEGG) database (<http://www.kegg.jp/kegg>) was used to enrich signaling pathways and perform function annotation. The bubble diagram was visualized using ggplot (R package).

## ROS Identification

Frozen tissue was cut into sections using a freezing microtome (Cryotome E, Thermo Fisher, China) that was returned to room temperature. A liquid blocker PAP pen (G6100, Servicebio, Wuhan) was utilized to draw a circle, preventing the antibody from escaping. The samples were mixed with a spontaneous fluorescence quenching agent for 8 min and stained using dihydroethidium (D7008, SIGMA, America) for 45 min at 37 °C in the dark environment. The sections were sealed with an anti-fluorescence quenching agent. Images were photographed with a forward fluorescence microscope (Nikon Eclipse C1, Nikon, Japan). DAPI-stained nuclei were blue under the excitation wavelength at 330 nm, and the positive-expression area was red. Image J software was employed to measure the relative positive rate of each image (image analysis was finished within 3 h to avoid fluorescence quenching). Each figure was measured 3 times under the same mode.

## Cytokines/Inflammation Medium Concentration Detection

The hypothalamus tissues were mixed with cold PBS at the ratio of 1:9 ( $w:v$ ) and homogenized to obtain the fresh supernatant, which was centrifuged at 4500  $r\cdot\text{min}^{-1}$  for 18 min, at 4 °C. The contents of IL-6, IL-10, tumor necrosis factor (TNF)- $\alpha$ , IFN- $\gamma$ , NO, and iNOS were detected using the specific enzyme-linked immunosorbent assay kits (Hengyuan, China). All procedures were consistent with the instructions. Finally, the optical density was measured at 550 nm (SpectraMax@ABS 00,254, MOLECULAR DEVICES, America) when the enzymatic reaction was stopped. The serum cytokines contents were calculated based on the standard curve drawn by ELISAcalc software.

## 16S Ribosomal RNA Gene (16S rDNA) Amplicon Sequencing

After the intravenous anesthesia was conducted, the porcine abdominal cavity was slit to ligature the jejunum region and the enteric content was collected with sterile tubes. Total DNA was extracted using the specialized kits and stored in refrigerator at -80 °C. After the chimeric sequences were filtered using the Vsearch 2.3.4 software, clean tags were demodulated and denoised based on DADA2 to purify the amplicon sequence variant feature sequences. Based on the Bayes ribosomal database project (RDP) classifier, the

public SILVA ribosomal RNA database (<http://www.arb-silva.de/>) was used to annotate the taxonomical classification of feature sequences for each operational taxonomic unit (OTU). Relative species abundances in each sample were normalized based on the amplicon sequence variant abundance accompanied with the Kruskal–Wallis test was used to compare the abundance difference. The detailed sequencing steps and bioinformatics analysis could refer to the previous literature published by our lab. The function of the microbiome taxa was predicted using the online PICRUSt2 program.

## Neurotransmitter Content Assay

In total, 200 mg fresh hypothalamus tissues were ground to obtain homogenate which was centrifuged for 12 min in the cold condition. Each sample well (including 50  $\mu\text{L}$  tissue supernatant and the mixture of 0.1% ascorbic acid and triketohydrindene hydrate) was heated in the boiling water bath and then cooled for 10 min. When the red-brown solution was replaced with violet, the absorbance value was measured at 330 nm wavelength using the enzyme-labeled instrument. The blank control group was also set. The relative glutamate content in the hypothalamus was calculated as followed:  $[\text{absorbance value (standard well)} / \text{absorbance value (measured well)}] \times \text{standard solution concentration (150 } \mu\text{mol}\cdot\text{L}^{-1})$ .

## Immunohistochemistry Analysis

Immune-related factors (IL-6, IL-10, and TNF- $\alpha$ ) and apoptosis-mediated indexes (Cyt C, P53, P38, and Caspase3) were analyzed by immunohistochemistry. Tissue paraffin sections were dewaxed with xylene and graded ethanol solutions were used for dehydration. Antigen repair was performed in citric acid antigen repair buffer in the microwave oven, which was followed by 3% hydrogen peroxide added into sections to block the endogenous peroxidase activity. The paraffin sections were covered with 3% bovine serum albumin solution and then incubated with primary antibodies (1:650 dilution) overnight. The next day, the horse-radish peroxidase-labelled secondary antibody (goat anti-rabbit IgG). A chromogenic agent was added to stop color development followed by redyeing with hematoxylin. Finally, the sections were dehydrated and sealed with neutral resin. The images were observed under a digital microscope. The nucleus was blue and the positive expression area of the target protein was brown. Image J 1.51 K software was used to detect the positive signals, and the positive rate of each image was counted.

## Terminal Deoxynucleotidyl Transferase-Mediated dUTP Nick-End Labeling Analysis

The paraffin sections above were dewaxed and then protease K and PBS-TRITON solution were added into the incubation box to be incubated in a dark place. Subsequently, terminal deoxynucleotidyl transferase, FITC-labeled 2'-deoxyuridine 5'-triphosphate

(dUTP), and labeling buffer were added to be incubated for 120 min to stain the apoptotic cells, respectively. After staining with DAPI dye liquor, an anti-fluorescence quenching mounting medium was used to seal sections. The images were photographed under the fluorescence microscope (Eclipse Ci-L, NIKON, Japan) and the apoptosis proportion was calculated using a relevant formula. The normal cells were blue and early-apoptotic cells showed green color. Each image was analyzed three times under the same parameters, and the average values of the quantitative results were recorded as the relative apoptosis rate.

### Real-Time Quantitative Polymerase Chain Reaction

In total, 100 mg hypothalamus tissue was mixed with 1000  $\mu\text{L}$  TRIzol reagent (204205, Thermo Fisher, China) and the mixture was ground fully at 4 °C for 7 min to release the total RNA. Then, trichloromethane was added to accelerate the separation of the organic phase-water phase and the supernatant was collected after centrifugation for 15 min. To precipitate the total RNA, an equal volume of isopropyl alcohol was mixed with the supernatant to leave to set for 10 min. After the RNA precipitate was rinsed two times using 75% ethanol-DEPC buffer, the concentration (850–1250  $\text{ng}\cdot\mu\text{L}^{-1}$ ) and purity (1.9–2.2) of the total RNA was measured and the total RNA was stored at –80 °C for the further experiment. The detailed procedures of reverse transcription, specific primer design, and fluorescence quantitative amplification were referred to in the previous literature published by our lab. The sequences of the primers used in the current experiment were shown in Table S2.

### Western Blot

Frozen tissue was ground with Western and IP lysis buffer (P0013, BEYOTIME, Shanghai) mixed with phenylmethylsulfonyl fluoride (ST506, BEYOTIME, Shanghai) and phosphatase inhibitor (04906837001, ROCHE, Switzerland) to prevent the degradation of total protein and phosphate groups. The concentration of total protein was quantified using the bicinchoninic acid protein assay kit (PC0020, SOLARBIO, Beijing) and diluted to 5–8  $\text{mg}\cdot\text{mL}^{-3}$ . Total protein was separated by the electrophoresis system with 10% sodium dodecyl sulfate–polyacrylamide gel for 105 min according to the molecular weight. Next, the total protein was transferred to the nitrocellulose filter membrane at 10 V, 350 mA for 45 min, and the membrane was blocked using 5% skim milk powder or bovine serum albumin (for phosphorylated protein). Finally, the membrane was incubated with corresponding primary antibodies (Table S3) for 18 h and then incubated with the horseradish peroxidase-conjugated goat anti-rabbit IgG (H&L) (RS0002, ImmunoWay, Beijing) for 95 min in dark. The signal was enhanced by the ultra-sensitive enhanced chemiluminescence substrate kit (HY-K1005, MCE, America) and the target bands were

detected using the chemiluminescence gel imaging analysis system (C300, AZURE BIOSYSTEMS, America). Each image was quantified three times using Image J software.

### Ultrastructure Observation

The hypothalamus tissue was cut into 1.0  $\text{mm}^3$  small blocks. After being fixed in 2.5% glutaraldehyde solution (No. 18426, TED PELLA, America) for 24 h, the tissue blocks were rinsed with 0.1 M phosphate-buffered saline (PBS) for 10 min, and this process was repeated 3 times. 1% osmic acid fixative (No. 18456, TED PELLA, America) was used to fix for 2 h. The tissue was rinsed 3 times and the tissue blocks were dehydrated with gradient ethanol solution. Then, the tissue was infiltrated with different proportions of epoxide resin (No. 1). Finally, the tissue was embedded and polymerized in the heat insulation box overnight. After being cut into sections in a thickness of 50 nm by the ultra-thin slicer (EM UC7, Leica, Germany), the sections were double-stained with uranyl acetate and lead citrate. The transmission electron microscopy (H7650, HITACHI, Japan) to observe the submicroscopic structure.

### Data Processing and Statistical Analysis

SPSS software (Version 24.0, SPSS INC., America) was used for statistical analysis. The normal distribution test was performed using the Kolmogorov–Smirnov method. Meanwhile, Levene's test was implemented to determine the homogeneity of variance. One-way analysis of variance (ANOVA) and post hoc test with Tukey's honestly significant difference method were performed to compare the statistical significance between each of the two groups. The statistical significance level in the present study was selected as 0.05. Bars with different lowercase meant a significant difference between the two groups ( $P$  value < 0.05). All indexes were shown as mean  $\pm$  standard deviation (SD). All figures in our results were visualized by MS Office 2021. The visualization process for transcriptome analysis and 16S rDNA amplicon sequencing were completed by the R studio package (Version 9.0.190312).

## Results

### Effects of Ammonia Poisoning on Neurotransmitter Levels

To investigate the effect of ammonia exposure on neurotransmitter secretion, glutamate content in the hypothalamus tissue was determined. As shown in Fig. S1, ammonia poisoning significantly inhibited glutamate synthesis and secretion in the hypothalamus ( $P$  < 0.05) and exogenous L-selenomethionine supplementation in basal diet could significantly restore glutamic acid levels in the hypothalamus ( $P$  < 0.05). However,

compared with the C group, there was no significant change in glutamate content in the Se group ( $P > 0.05$ ).

### Effect of Ammonia Poisoning on Selenium Content in Tissues

The Se content in the hypothalamus tissues was evaluated by inductively coupled plasma mass spectrometry (ICP-MS), and the results were expressed in the form of heat maps. As shown in Fig. S2, compared with the C group, the Se content in the tissues decreased after ammonia exposure for 30 days, but the difference was not statistically significant ( $P > 0.05$ ). Compared with the C group, the content of Se in the Se group was significantly increased ( $P < 0.05$ ); Compared with the A group, the Se content in the A+Se group increased but was lower than in the Se group ( $P < 0.05$ ).

### Effect of Excessive Ammonia on Growth Performance and Meat Quality

Growth performance is an important index reflecting the effect of ammonia exposure on animals. The body weight of finishing pigs in all groups increased, but the weight gain in the A group was the least in Table S4. There were no significant differences in ADG and FC indexes in each group ( $P > 0.05$ ), while there was a significant difference in FI indexes between the C group and the A group ( $P < 0.05$ ).

In addition to growth performance, meat quality is also an important index reflecting the effects of ammonia on animals (Table S5). There were no significant differences in pH value, b\*, and SH indexes among all groups ( $P > 0.05$ ). There were significant differences in L\* and a\* indexes between the A group and the other groups ( $P < 0.05$ ). There were significant differences in DS indexes between the C group and the A group ( $P < 0.05$ ).

### Effect of Excessive Ammonia on pathological symptoms of Fattening Pigs

The pathological symptoms of experimental animals were observed, and the results were shown in Fig. 1. Compared with the C group, the degree of activity in the A group was

significantly decreased ( $P < 0.05$ ). Meanwhile, compared with the A group, the foraging desire and degree of activity increased in the A+Se group, but there was no statistical difference in feeding desire between the A group and the A+Se group ( $P > 0.05$ ). These results indicated that ammonia poisoning reduced foraging desire and degree of activity in pigs.

### Enrichment Analysis for Signaling Pathways

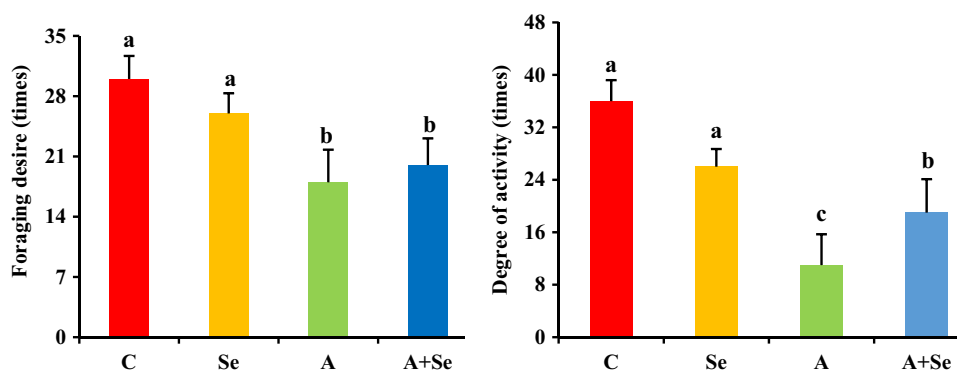
KEGG pathway enrichment results were shown in Fig. 2a. In the hypothalamus, all differentially expressed genes corresponded to 248 KEGG pathways (33 significant) and 231 GO pathways (27 significant), respectively. Among the first 20 KEGG pathways in the hypothalamus, immune-related pathways include “T cell receptor signaling pathway”, “Th1 and Th2 cell differentiation”, “Th17 cell differentiation”, “primary immune deficiency”, “human T-cell leukemia virus 1 infection”, “cell adhesion molecule”, and “human immunodeficiency virus 1 infection”. It was also found that ammonia treatment could significantly regulate the cAMP signaling pathway in the hypothalamus.

KEGG database was also used to predict the changes in the biological functions of intestinal flora in the A group and the A+Se group (Fig. 2b). In the biological oxidation process, the average proportion of “glyceraldehyde-3-phosphate dehydrogenase, type I” pathway in the A+Se group was up-regulated ( $P < 0.05$ ).

### Effect of Ammonia Poisoning on Inflammatory Indexes Levels

The changes in inflammatory indexes in the hypothalamus were shown in Fig. 3. Compared with the C group, the activity of iNOS and NO content significantly increased by 138.81% and 102.06% after ammonia exposure, respectively ( $P < 0.05$ ). Compared with the A group, the two inflammatory indexes in the A+Se group were significantly decreased (the levels of iNOS and NO decreased 40.38% and 42.41%, respectively) ( $P < 0.05$ ), but still significantly higher than the C group ( $P < 0.05$ ). In addition, the relative protein expression of iNOS in the A group was significantly higher than that in the C group. The protein expression of iNOS in the A+Se group was significantly lower than that in the

**Fig. 1** Observation of pathological symptoms. Data in each group were described as mean  $\pm$  SD. Bars with different lowercase represent statistical significance ( $P < 0.05$ ) between two groups ( $n = 6$ )



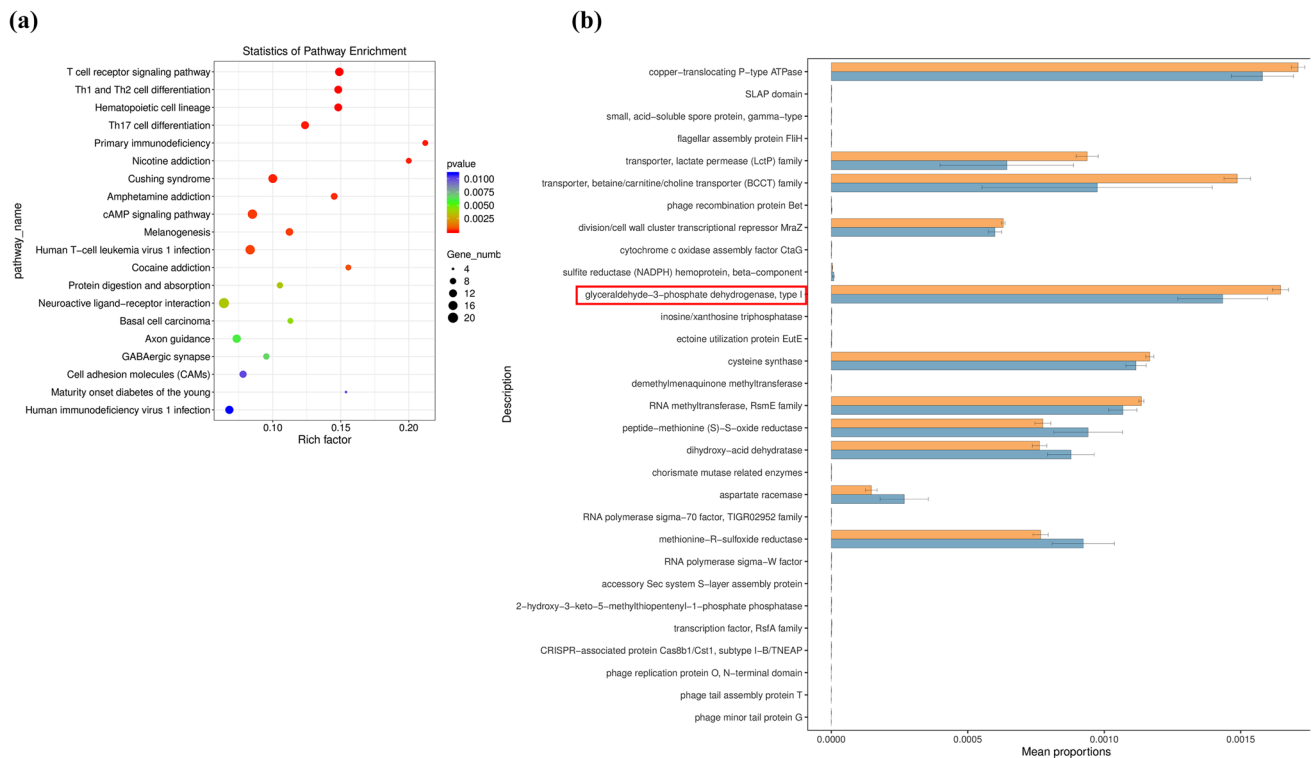


**Fig. 2** Multiple omics analysis. **a** Bubble diagram for Kyoto Encyclopedia of Genes and Genomes (KEGG) enrichment analysis. The size of nodes indicated the gene number which mapped to the GO term. Color represented  $P$  value decreased from left to right. X-coor-

dinate represented the relative rich factors of each KEGG pathway. **b** Function prediction analysis for gut microbiota based on the KEGG database. Blue represented the A group while orange represented the A+Se group

A group ( $P < 0.05$ ), but the iNOS protein level in the A+Se group was still significantly higher than that in the C group ( $P < 0.05$ ).

The contents of cytokines (TNF- $\alpha$ , IFN- $\gamma$ , IL-6, and IL-10) in the hypothalamus were detected by ELISA to evaluate the effects of ammonia poisoning on the immune indexes of finishing pigs. The results were shown in Fig. 3. Compared with the C group, the contents of IL-6, IL-10, and TNF- $\alpha$  in the A group were significantly increased ( $P < 0.05$ ), while IFN- $\gamma$  levels were significantly decreased ( $P < 0.05$ ). For the hypothalamus, the contents of TNF- $\alpha$ , IL-6, and IL-10 in the A+Se group were significantly decreased compared with those in the A group ( $P < 0.05$ ), and IFN- $\gamma$  content was significantly increased ( $P < 0.05$ ). Except for IL-6, there was no significant difference in the contents of other cytokines between the C group and the Se group ( $P > 0.05$ ).

### Effects of Ammonia Poisoning on the Relative ROS Level

The distribution of ROS in tissues was shown in Fig. 4. Compared with the C group and the Se group, the positive rate of ROS in the hypothalamus tissue of finishing pigs was significantly increased under high ammonia environment stimulation ( $P < 0.05$ ). The abnormal accumulation

of intracellular ROS induced by high ammonia stimulation could be alleviated by adding L-selenomethionine in the basal diet, and ROS content in tissues was reduced. The ROS positive rate in the hypothalamus in the A+Se group was significantly higher than that in the C group ( $P < 0.05$ ), indicating that Se only could inhibit ROS accumulation to a certain extent.

### Effect of Ammonia Poisoning on Sub-microstructure

The sub-microstructure of hypothalamus tissue was shown in Fig. 5. In the C group and Se group, the cell structure was intact without obvious pathological changes and electron density was uniform. The boundary of the nuclear membrane (M) was neat while chromatin (C) in the nucleus was evenly distributed. The mitochondrial (MI) structure was complete, the crest structure was clear, and the double membrane structure was obvious. In the A group, chromatin (C) was agglutinated and heterochromatin increased significantly in the hypothalamus cells. The nuclear membrane (M) was folded and shrunken, and some nuclear membranes were broken. Nucleolar ambiguity; Severe fracture of mitochondrial (MI) crest; The

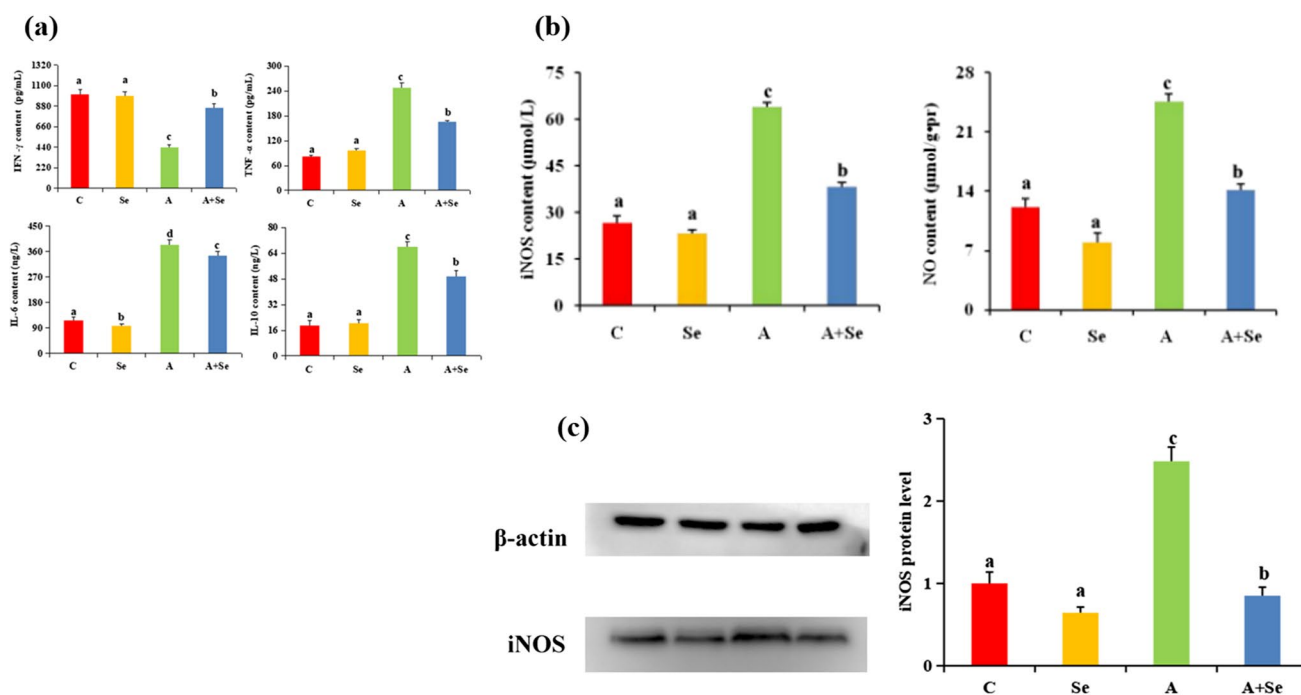


**Fig. 3** The effect of excessive ammonia stimulation on the inflammatory indicators. Data in each group were described as mean  $\pm$  SD. Bars with different lowercase represent statistical significance

( $P < 0.05$ ) between two groups ( $n = 6$ ). **a** The contents of inflammatory cytokines. **b** The iNOS activity and NO content in the hypothalamus. **c** The protein expression level of iNOS

presence of apoptotic bodies (AB) was also observed. In the A + Se group, part of chromatin (C) was still marginal

in hypothalamus cells. The nuclear membrane (M) shape was irregular; Some mitochondria (MI) showed obvious

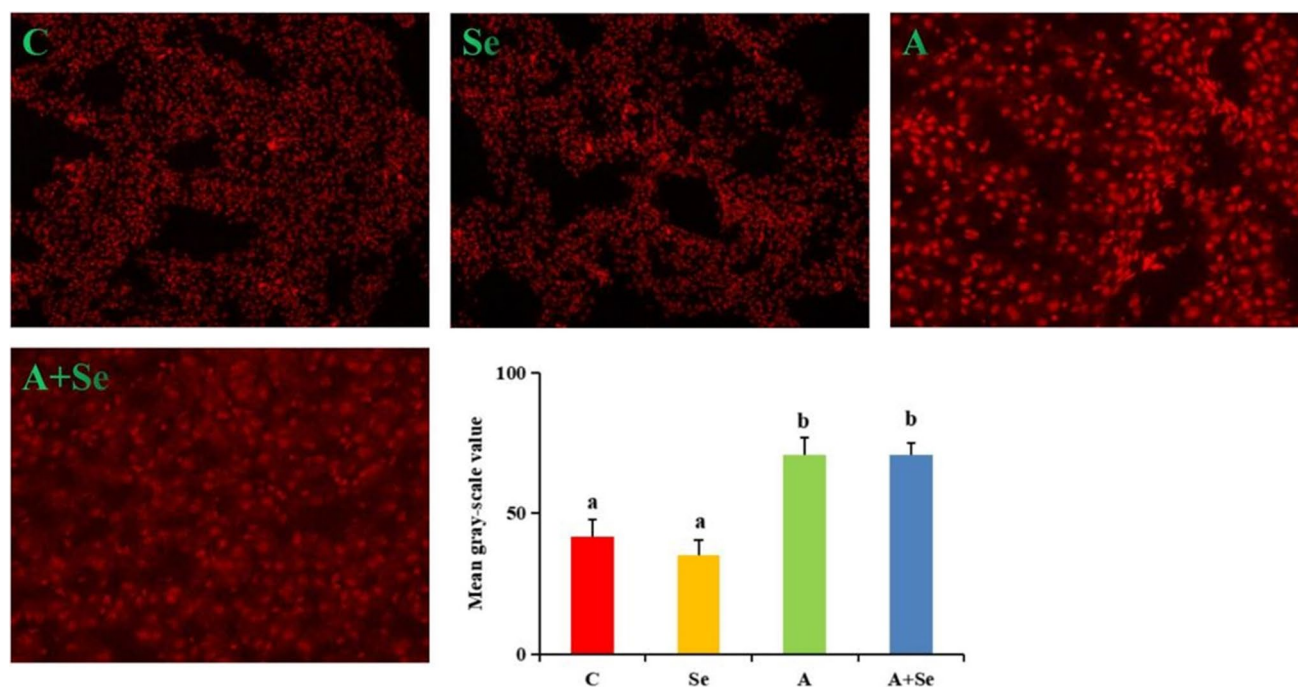
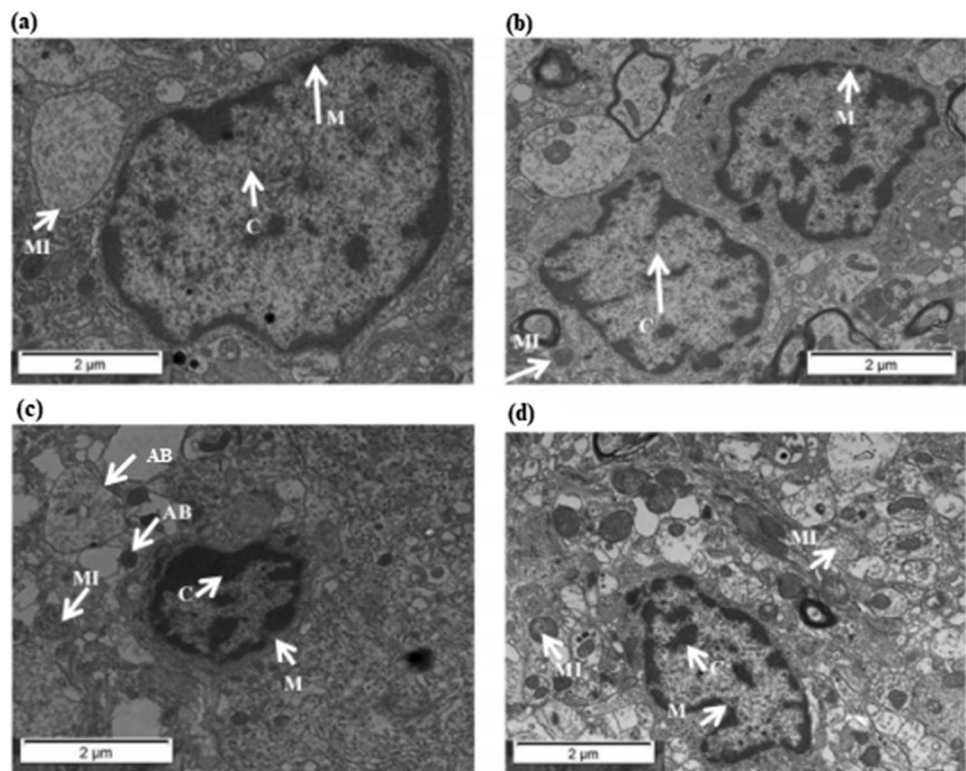


**Fig. 4** The effect of excessive ammonia stimulation on the ROS content in the hypothalamus. Data in each group were described as mean  $\pm$  SD. Bars with different lowercase represent statistical significance ( $P < 0.05$ ) between two groups ( $n = 6$ )



**Fig. 5** The effect of excessive ammonia stimulation on the ultrastructure changes in the hypothalamus. **a** C group, 10,000 $\times$ ; **b** Se group, 10,000 $\times$ ; **c** A group, 10,000 $\times$ ; **d** A + Se group, 10,000 $\times$



crest fracture, but the fracture degree was significantly relieved compared with the A group.

### Effect of Ammonia Exposure on the Cell Apoptosis Rate

In order to investigate the effect of ammonia poisoning on cell apoptosis, the positive rate of apoptotic cells was detected by terminal DNA transferase dUTP notch terminal labeling (TUNEL) analysis. The results were shown in Fig. 6. The apoptotic cells in the hypothalamus in the A group were significantly higher than those in the C group ( $P < 0.05$ ). Compared with the A group, the apoptotic positive cells in the A + Se group were significantly decreased ( $P < 0.05$ ), but still higher than that in the C group and the Se group ( $P < 0.05$ ). There was no significant difference between the Se group and the C group ( $P > 0.05$ ).

### Immunohistochemical Analysis

The content of apoptosis-related proteins (Caspase3, Cyt C, P53, and P38) and immune-related proteins (IL-10, IL-6, and TNF- $\alpha$ ) in the hypothalamus were quantitatively analyzed by immunohistochemical positive signal detection. The target proteins were stained brown (Fig. S3) and the quantitative results were shown in Table S6. Except for IL-6, ammonia poisoning significantly increased the protein levels of four apoptosis-inducing factors and three immune

factors in the hypothalamus ( $P < 0.05$ ). It was also found that L-selenomethionine could alleviate the over-expression of apoptosis-related proteins and immune-related proteins induced by ammonia poisoning ( $P < 0.05$ ).

### Effects of Ammonia Exposure on the Apoptosis Signaling Pathway

Based on the results of the KEGG pathway enrichment analysis, the expression levels of core proteins in the apoptosis-related signaling pathway (PI3K/Akt/PPAR- $\gamma$ ) were detected (Fig. 7). Compared with the C group, the overexpression of pro-apoptotic proteins (Cyt C, Caspase3, Caspase9, and Bax) were significantly augmented after 30 d of ammonia exposure ( $P < 0.05$ ). Meanwhile, the levels of anti-apoptotic proteins (PI3K, Akt, PPAR- $\gamma$ , p-PI3K, and p-Akt) in the A group were significantly lower than those in the other three groups ( $P < 0.05$ ). There was no significant difference in protein levels between the C group and Se group at protein levels ( $P > 0.05$ ). Compared with the A group, the protein levels of anti-apoptotic factors (PI3K, Akt, p-PI3K, and p-Akt) were significantly up-regulated in the A + Se group ( $P < 0.05$ ), and the expression of pro-apoptotic proteins (Cyt C, Caspase3, Caspase9, and Bax) was inhibited. Except for Akt and p-Akt, other protein levels in the A + Se group were significantly different from those in the C group ( $P < 0.05$ ). The mRNA levels of these

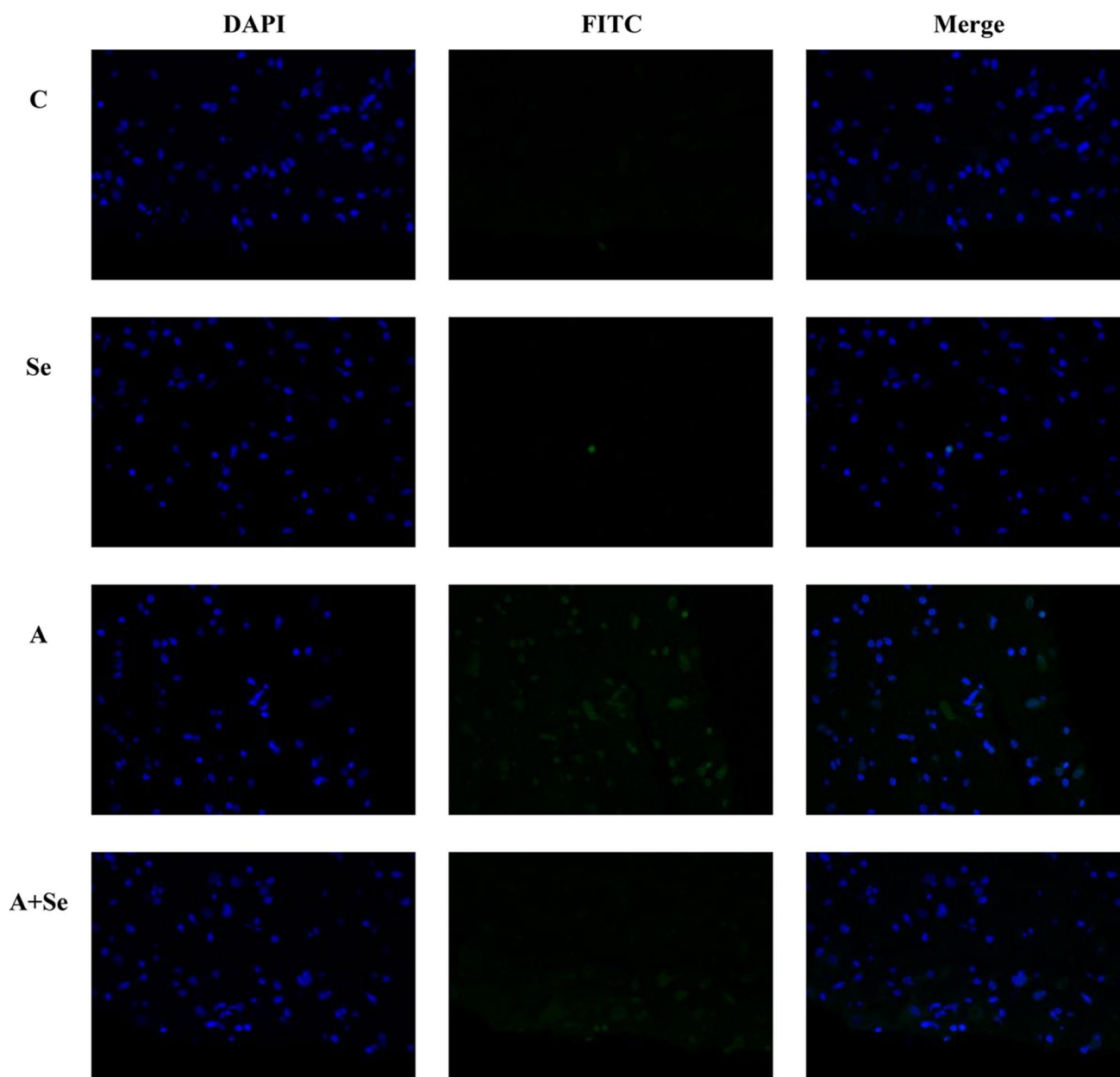


**Fig. 6** The effect of excessive ammonia stimulation on the ratio of apoptotic cells in the hypothalamus. Green represented the positive apoptosis cells while blue represented the nucleus

apoptosis-related genes had a similar change trend to the protein levels (Fig. S6).

#### Effects of Ammonia Poisoning on Expression Levels of Mitochondrial Dynamics-Related Factors

In this study, the mRNA relative levels of mitochondrial fusion genes (OPA1, Mfn1, Mfn2) and mitochondrial fission genes (Drp1, Mff) in the hypothalamus were detected and shown in Fig. S4. Compared with the C group, the

genes of OPA1, Mfn1 and Mfn2 in the A group were significantly down-regulated ( $P < 0.05$ ), while Drp1 and Mff genes were significantly up-regulated ( $P < 0.05$ ). Compared with the A group, the mRNA levels of OPA1, Mfn1, and Mfn2 in the A + Se group were increased ( $P < 0.05$ ), and the mRNA levels of Drp1 and Mff were significantly decreased ( $P < 0.05$ ). Compared with the C group, the mRNA level of the Mfn1 gene in the Se group was significantly increased ( $P < 0.05$ ).

The protein expression level of each gene (Fig. S5) showed the same trend as the mRNA level. There was no

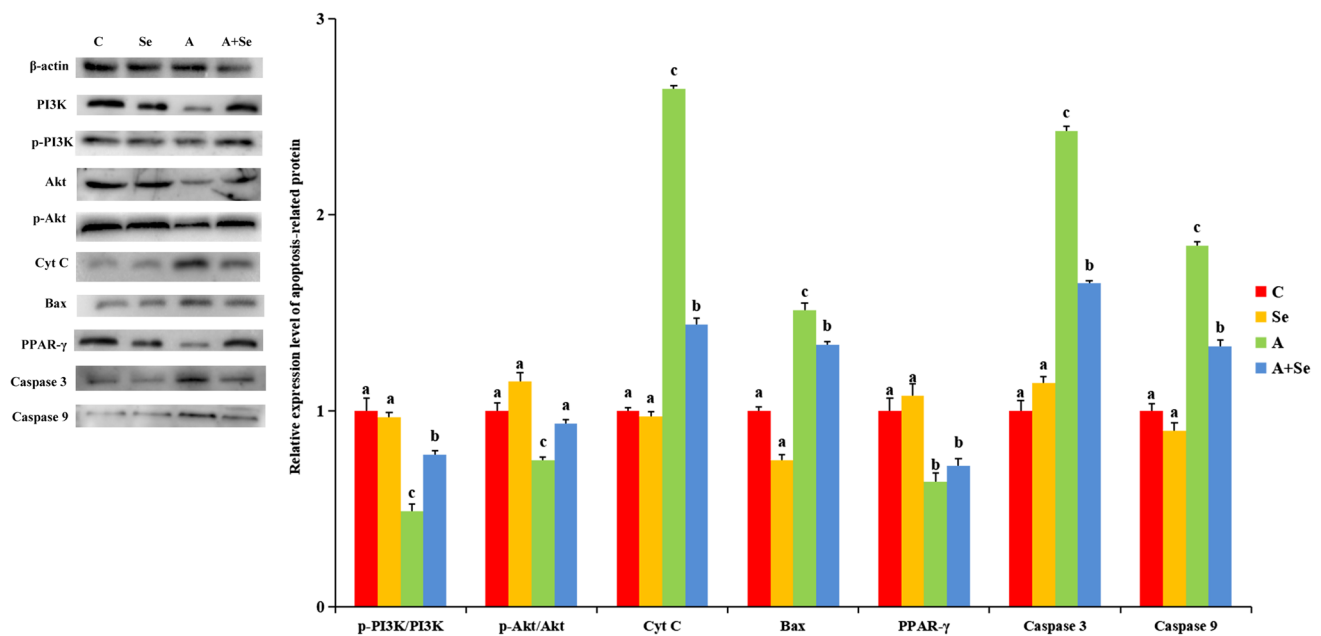


**Fig. 7** The expression level of apoptosis-related proteins in the hypothalamus. Data in each group were described as mean  $\pm$  SD. Bars with different lowercase represent statistical significance ( $P < 0.05$ ) between two groups ( $n = 6$ )

significant difference in the expression levels of each protein (except for Mfn1) in the Se group compared with the C group ( $P > 0.05$ ). In addition, compared with the A group, the protein level of mitochondrial fusion-related factors (except for Mfn1 and Mfn2) was significantly increased in the A + Se group ( $P < 0.05$ ). Except for OPA1 protein, the levels of all proteins in the A + Se group were significantly different from those in the C group ( $P < 0.05$ ).

## Discussion

Philips et al. found that ammonia exposure increased the duration of the lying behavior of the bulls, indicating ammonia inhalation could decrease animal excitability [40]. Consistent with previous results, in our study, ammonia poisoning also caused the attenuation of activeness in fattening pigs and inhibited the synthesis of glutamate in the hypothalamus. Under the condition of ammonia poisoning, free ammonium ion was synthesized to glutamine [41], which might elevate the oncotic pressure of neurons and then inhibit the secretion of excitatory neurotransmitters. Finally, the excitement transmission between synapses was blocked to affect the activity degree of organisms. Consistent with previous conclusions [42], the present study also found high ammonia environment inhibited the foraging desire of fattening pigs. Animals need to depend on the sight, taste, and smell of sensory organs to obtain food [43]; however, excessive ammonia would stimulate the eye and respiratory mucosa, affecting the perception of foods to attenuate the

foraging motivation [44]. In addition, ammonia showed alkaline characteristics when dissolved in water, making pigs feel indisposed when chewing the diet to weaken the foraging desire.

Ammonia exposure could decrease food intake, which deprived the protein and energy intake. The intake of nutrients could affect the ratio of the oxidized muscle fiber to fat content, which reduced the meat quality [45]. Ammonia stimulation caused changes in glycogen content, which altered the pH value of muscle. A previous study found that ammonia exposure could decrease the pH value/ tenderness of chest muscle and augment the trend of drip loss [46]. In addition, pectoral muscle  $b^*$ ,  $L^*$ , and shear forces of broilers were elevated after chronic ammonia exposure [46]. In our study, these typical meat quality indexes had similar results to the previous literature [47], indicating ammonia poisoning had negative effects on the meat quality of fattening pigs. Consistent with our results, the original studies demonstrated that the ADG and FI were significantly decreased after chronic ammonia inhalation [47], indicating a high concentration of ammonia inhibited the foraging motivation to decrease the porcine growth performance.

As an acute phase reactive protein, IL-6 could promote inflammation development [48, 49] and the differentiation of immune cells to elevate the defense ability against xenobiotics. IFN- $\gamma$  could decrease the level of TNF- $\alpha$  by inhibiting the nuclear factor kappa beta pathway [50]. Wang et al. found that excessive ammonia enhanced the mRNA level of IL-6 and neutrophil infiltration was observed in chicken jejunum [51]. A previous study also reported that hydrogen

sulfide inhalation could decrease the IFN- $\gamma$  transcriptional level in lung tissue and cause inflammatory cell aggregation [52]. In our study, the changes in the contents of IL-6 and IFN- $\gamma$  indicated that humoral immunity had predominance in the immune system after ammonia poisoning and then the inflammation response was initiated. TNF- $\alpha$  could aggravate tissue inflammation and promote the formation of cellular peroxide anion. Ammonia inhalation stress would increase the expression of TNF- $\alpha$  in the respiratory tract, heart, and liver, which was accompanied by inflammatory injury [15, 53]. IL-10 had double response models in inflammation response, namely IL-10 could inhibit or promote inflammation occurrence. IL-10 could inhibit T cell to perform immune functions by blocking the secretion of IFN- $\gamma$ , inhibiting the inflammation defense [54]. In the present study, the TNF- $\alpha$  and IL-10 levels in the hypothalamus increased and lymphocyte aggregation was observed [32], indicating that ammonia poisoning could accelerate inflammation development by the formation of peroxide anion and then the accumulated IL-10 inhibited the initiation of the immune program. IFN- $\gamma$  could be regarded as a highly effective inducer of NO, but a high level of NO interfered with the expression of IFN- $\gamma$  in turn [55]. Xing et al. found excessive ammonia inhalation activated iNOS activity through the miR-202-5p/PTEN pathway, inducing the continuous synthesis of NO [56]. In our study, the NO content and iNOS activity were up-regulated, which indicated that ammonia inhalation would initiate the spontaneous inflammatory response, subsequently, the synthesis of the cytokines related to inflammation were regulated to cause the target organs injury.

Gut microbiota is usually related to physiological metabolic activities. In our existing research [57], the pathways related to biological oxidation and amino acid metabolism were significantly altered after chronic ammonia exposure. Combined with the results in the current study, it showed that organisms initiated the endogenous compensatory mechanisms after ammonia poisoning and destroyed the energy metabolism balance to regulate the inflammation response process. Our previous study also found that organic Se supplement would enhance the abundance of *Lactobacillus* [57]. As one kind of beneficial bacteria, *Lactobacillus* participated in energy metabolism to inhibit excessive energy consumption in organisms [58]. Above all, L-selenomethionine might relieve the toxicity effects induced by ammonia exposure by blocking gut microbiota-driven energy metabolism disturbance.

Excessive ammonia could destroy the mitochondrial structure through oxidative stress to activate the mitochondria-mediated apoptosis pathway [59]. Mitochondrial homeostasis included the fusion and fission of the mitochondrial membrane. As two mitochondrial fission-related factors, dynamin-related protein1 (Drp1) and mitochondrial fission factor (Mff) could accelerate the fragmentation of mitochondria and

promote the transmission of Cyt C to cytoplasm, activating the Caspase family members to mediate cell apoptosis [60]. Mitochondrial fusion inhibition could be regarded as a main inducement of apoptosis. Mitochondrial fusion protein (Mfn) 1 and Mfn2 could promote the fusion of the mitochondrial outer membrane while optic atrophy (OPA) 1 accelerated the fusion of the mitochondrial inner membrane [61]. Excessive ammonia caused the disturbance of mitochondrial dynamics proteins and cell apoptosis in the kidney [62]. In our study, ammonia exposure caused abnormal expression levels of mitochondrial dynamics factors accompanied by mitochondrial crest fracture and promoted the formation of an apoptotic body. Meanwhile, the ROS density in the cell was elevated after chronic ammonia exposure. These results demonstrated that ammonia poisoning mediated the imbalance of mitochondrial dynamics to cause mitochondria injury and oxidative stress response, inhibiting ATP synthesis to induce cell apoptosis. P53 is one checkpoint for G1 phase division and an important apoptotic inducer [63]. P53 can inhibit the expression of B cell lymphoma/Leukemia-2 (Bcl-2) to promote the transcription of Bcl-2 associated X (Bax) indirectly, which would accelerate cell apoptosis [64]. Subsequently, apoptotic protease activating factor-1 (Apaf-1), Cyt C, and Caspase3 were anchored to form an apoptotic body, inducing the cell apoptosis finally (Figure S7). Many signaling pathways are involved in the regulation of the apoptosis process, such as the phosphoinositide 3-kinase (PI3K)/protein kinase B (Akt)/peroxisome proliferator-activated receptor (PPAR- $\gamma$ ) axis. PPAR- $\gamma$ , which could inhibit cell-programmed apoptosis, is an upstream regulatory element of cyclooxygenase 2 [52]. The expression level of PPAR- $\gamma$  was suppressed in the porcine kidney under cadmium exposure and the typical characteristics of apoptosis were observed [65]. So far, it has been demonstrated that cadmium could induce the apoptosis of pancreas cells in chickens by suppressing the PI3K/Akt/PPAR- $\gamma$  pathway while the pro-apoptosis factors were up-regulated [66]. In the present study, the levels of PI3K, p-PI3K, Akt, p-Akt, and PPAR- $\gamma$  were decreased while Caspase3, Bax, and Cyt C were up-regulated. Our study proved that the PI3K/Akt/PPAR- $\gamma$  axis was blocked after ammonia poisoning, activating the mitochondria-mediated apoptosis pathway to accelerate the cell apoptosis process. In addition, we found that the P38 level was augmented after excessive ammonia inhalation. Previous literature also reported that ROS could promote the expression of P38 and then mediate cell apoptosis [67]. Our results demonstrated that ammonia inhalation induced oxidative stress to promote the synthesis of P38, regulating the apoptosis-related pathways to accelerate apoptosis process.

Se can inhibit ROS accumulation to avoid the increasing trend of mitochondrial calcium, protecting the nucleosome DNA to suppress the abnormal apoptosis process. Han et al. found that organic Se decreased oxidative stress to inhibit

endoplasmic reticulum stress-mediated apoptosis in the porcine kidney after ammonia exposure [68]. In our study, L-selenomethionine activated the PI3K/Akt/PPAR- $\gamma$  axis to inhibit the mitochondrial apoptosis pathway by promoting the phosphorylation process of PI3K and Akt, in parallel, organic Se could restore mitochondrial dynamics homeostasis to alleviate the ammonia poisoning-induced mitochondria injury and cell apoptosis. In addition, Se could enhance the chemotaxis of neutrophil activity to inhibit inflammation development. According to related literature, sodium selenite alleviated cadmium poisoning-mediated immune imbalance and inflammation injury [69]. In our study, the organic Se supplement altered the levels of inflammatory mediators and decreased ROS accumulation, indicating that Se could inhibit the inflammation to alleviate the neurotoxicity of excessive ammonia inhalation by regulating the oxidative stress level. Meanwhile, Se is involved in neural development, which has the benefits to repair the damaged neuron, restoring the foraging desire and activeness in fattening pigs after ammonia poisoning. Interestingly, we found exogenous Se supplement could enhance Se content in tissue, which was consistent with previous reports [70]. It was speculated that exogenous L-selenomethionine could be absorbed into an intracellular fluid to play normal physiological effects. Additionally, ammonia exposure might not cause the Se content disorder in the hypothalamus. The detailed mechanisms still need to be further clarified.

## Conclusion

A high concentration of atmospheric ammonia showed extrinsic neurotoxicity to fattening pigs by promoting the programmed apoptosis process mediated by the mitochondrial dynamics dysfunction. Meanwhile, ammonia inhalation could accelerate the inflammation development through the occurrence of Th1/Th2 shift and the jejunal microbe taxa-driven metabolic disturbance. Supplementation with organic Se could attenuate the physiological injury induced by ammonia poisoning by repairing the mitochondria deformation to inhibit the inflammatory damage. Taken together, L-selenomethionine could be regarded as one effective chemical prophylactic substance to protect organisms from the toxicity of xenobiotics.

**Abbreviations** *Caspase*: Cysteine-specific proteinase; *TNF- $\alpha$* : Tumor necrosis factor- $\alpha$ ; *Cyt C*: Cytochrome c; *P38*: P38 MAPK; *P53*: Tumor protein p53; *Drp1*: Dynamin-related protein1; *Mff*: Mitochondrial fission factor; *Mfn1*: Mitochondrial fusion protein; *OPA1*: Optic atrophy1; *Apaf-1*: Apoptotic protease activating factor-1; *PPAR*: Peroxisome proliferator-activated receptor; *Akt*: Protein kinase B; *PI3K*: Phosphoinositide 3-kinase; *Se*: Selenium; *Th*: Helper T cell; *IL*: Interleukin; *IFN*: Interferon; *iNOS*: Inducible nitric oxide synthase; *NO*: Nitric oxide; *IgG*: Immunoglobulin- $\gamma$ ; *ROS*: Reactive oxygen species; *ICP-MS*: Inductively coupled plasma mass spectrometry;

*ADG*: Average daily gain; *FC*: Feed conversion ratio; *FI*: Daily feed intake; *WI*: Initial weight; *WF*: Final weight; *DS*: Drip loss efficiency; *dUTP*: 2'-Deoxyuridine 5'-triphosphate; *PBS*: Phosphate buffered saline

**Supplementary Information** The online version contains supplementary material available at <https://doi.org/10.1007/s12011-022-03434-w>.

**Acknowledgements** The study was supported by the China Agriculture Research System of MOF and MARA (Project No. CARS-35-05B). All authors would thank Lian Chuan-Biotechnology Co., Ltd (Hangzhou, China) for their assistance during the multi-omics analysis and the support of the Animal welfare and healthy breeding team at Northeast Agricultural University. The first author gives sincere gratitude to Dr. Huan Wang for her encouragement and cooperation during the period of master career.

**Author Contribution** Yutao Li: writing—original draft, methodology, investigation, formal analysis, data curation. Jing Wang: writing—review and editing, investigation, formal analysis, animal breeding, conceptualization. Houjuan Xing: methodology, investigation, language revision. Jun Bao: supervision, writing—review and editing, project administration, funding acquisition. All authors read and approved the final manuscript.

**Data Availability** Original data used and generated in this study are available from the corresponding author on request with a completed Data Transfer Agreement. The raw sequencing files can be obtained through the National Center for Biotechnology Information website (Accession No. PRJNA741846).

## Declarations

The Animal Ethics Committee of Northeast Agricultural University approved all procedures in the present experiment (No. NAU-MO-2021-021).

**Conflict of Interest** The authors declare no competing interests.

## References

1. Wang J, Li Y, Wang J, et al. (2022) Selenium alleviates ammonia-induced splenic cell apoptosis and inflammation by regulating the interleukin family-death receptor axis and Nrf2 signaling pathway. *Biol Trace Elem Res*. <https://doi.org/10.1007/s12011-022-03279-3>
2. Hayes ET, Curran TP, Dodd VA (2006) Odour and ammonia emissions from intensive poultry units in Ireland. *Bioresour Technol* 97:933–939. <https://doi.org/10.1016/j.biortech.2005.04.024>
3. Xing H, Luan S, Sun Y et al (2016) Effects of ammonia exposure on carcass traits and fatty acid composition of broiler meat. *Anim Nutr* 2:282–287. <https://doi.org/10.1016/j.aninu.2016.07.006>
4. Mihina S, Sauter M, Palkovicova Z et al (2012) Concentration of harmful gases in poultry and pig houses. *Anim Sci Pap Rep* 30:395–406
5. Artífano B, Pujadas M, Alonso-Blanco E et al (2018) Real-time monitoring of atmospheric ammonia during a pollution episode in Madrid (Spain). *Atmos Environ* 189:80–88. <https://doi.org/10.1016/j.atmosenv.2018.06.037>
6. Krupa SV (2003) Effects of atmospheric ammonia (NH<sub>3</sub>) on terrestrial vegetation: a review. *Environ Pollut* 124:179–221. [https://doi.org/10.1016/S0269-7491\(02\)00434-7](https://doi.org/10.1016/S0269-7491(02)00434-7)
7. Olivier JGJ, Bouwman AF, Van der Hoek KW et al (1998) Global air emission inventories for anthropogenic sources of NO<sub>x</sub>, NH<sub>3</sub>

- and N<sub>2</sub>O in 1990. *Environ Pollut* 102:135–148. [https://doi.org/10.1016/S0269-7491\(98\)80026-2](https://doi.org/10.1016/S0269-7491(98)80026-2)
8. Zhou S, Zhang X, Qin F et al (2022) The use of selenomethionine to reduce ammonia toxicity in porcine spleen by inhibiting endoplasmic reticulum stress and autophagy mediated by oxidative stress. *Ecotox Environ Safe* 242:113887. <https://doi.org/10.1016/j.ecoenv.2022.113887>
  9. Miles DM, Miller WW, Branton SL et al (2006) Ocular responses to ammonia in broiler chickens. *Avian Dis* 50:45–49. <https://doi.org/10.1637/7386-052405R.1>
  10. Smith JH, Wathes CM, Baldwin BA (1996) The preference of pigs for fresh air over ammoniated air. *Appl Anim Behav Sci* 49:417–424. [https://doi.org/10.1016/0168-1591\(96\)01048-9](https://doi.org/10.1016/0168-1591(96)01048-9)
  11. Skowronska M, Albrecht J (2013) Oxidative and nitrosative stress in ammonia neurotoxicity. *Neurochem Int* 62:731–737. <https://doi.org/10.1016/j.neuint.2012.10.013>
  12. Zeng X, Liu R, Li Y et al (2021) Excessive ammonia inhalation causes liver damage and dysfunction by altering gene networks associated with oxidative stress and immune function. *Ecotox Environ Safe* 217:112203. <https://doi.org/10.1016/j.ecoenv.2021.112203>
  13. Simsek S, Yildirim V, Cim A et al (2016) Serum IL-4 and IL-10 levels correlate with the symptoms of the drug-naïve adolescents with first episode, early onset schizophrenia. *J Child Adol Psychop* 26:721–726. <https://doi.org/10.1089/cap.2015.0220>
  14. Wang S, Cao Y, Wang S et al (2020) DEHP induces immunosuppression through disturbing inflammatory factors and CYPs system homeostasis in common carp neutrophils. *Fish Shellfish Immun* 96:26–31. <https://doi.org/10.1016/j.fsi.2019.11.073>
  15. Shi Q, Wang W, Chen M et al (2019) Ammonia induces Treg/Th1 imbalance with triggered NF-κB pathway leading to chicken respiratory inflammation response. *Sci Total Environ* 659:354–362. <https://doi.org/10.1016/j.scitotenv.2018.12.375>
  16. Aggarwal BB, Shishodia S, Sandur SK et al (2006) Inflammation and cancer: how hot is the link? *Biochem Pharmacol* 72:1605–1621. <https://doi.org/10.1016/j.bcp.2006.06.029>
  17. Liu S, Xu F, Fu J et al (2015) Protective roles of selenium on nitric oxide and the gene expression of inflammatory cytokines induced by cadmium in chicken splenic lymphocytes. *Biol Trace Elem Res* 168:252–260. <https://doi.org/10.1007/s12011-015-0354-z>
  18. An Y, Xing H, Zhang Y et al (2019) The evaluation of potential immunotoxicity induced by environmental pollutant ammonia in broilers. *Poultry Sci* 98:3165–3175. <https://doi.org/10.3382/ps/pez135>
  19. Berg RD (1996) The indigenous gastrointestinal microflora. *Trends Microbiol* 4:430–435. [https://doi.org/10.1016/0966-842x\(96\)10057-3](https://doi.org/10.1016/0966-842x(96)10057-3)
  20. Fung TC, Olson CA, Hsiao EY (2017) Interactions between the microbiota, immune and nervous systems in health and disease. *Nat Neurosci* 20:145–155. <https://doi.org/10.1038/nn.4476>
  21. Van der Waaij D, Berghuis-de Vries J, Lekkerkerk-Van der Wees J (1971) Colonization resistance of the digestive tract in conventional and antibiotic-treated mice. *Epidemiol Infect* 69:405–411. <https://doi.org/10.1017/s0022172400021653>
  22. Zarrinpar A, Chaix A, Yooseph S et al (2014) Diet and feeding pattern affect the diurnal dynamics of the gut microbiome. *Cell Metab* 20:1006–1017. <https://doi.org/10.1016/j.cmet.2014.11.008>
  23. Heijtz RD, Wang S, Anuar F et al (2011) Normal gut microbiota modulates brain development and behavior. *PNAS* 108:3047–3052. <https://doi.org/10.1073/pnas.1010529108>
  24. Brisbin JT, Gong J, Sharif S (2008) Interactions between commensal bacteria and the gut-associated immune system of the chicken. *Anim Health Res Rev* 9:101–110. <https://doi.org/10.1017/S146625230800145X>
  25. Ren Z, Wang H, Cui G et al (2021) Alterations in the human oral and gut microbiomes and lipidomics in COVID-19. *Gut* 70:1253. <https://doi.org/10.1136/gutjnl-2020-323826>
  26. Wingender G, Stepniak D, Krebs P et al (2012) Intestinal microbes affect phenotypes and functions of invariant natural killer T cells in mice. *Gastroenterology* 143:418–428. <https://doi.org/10.1053/j.gastro.2012.04.017>
  27. Caputi V, Marsilio I, Filpa V et al (2017) Antibiotic-induced dysbiosis of the microbiota impairs gut neuromuscular function in juvenile mice. *Brit J Pharmacol* 174:3623–3639. <https://doi.org/10.1111/bph.13965>
  28. Savitskaya M, Onishchenko G (2015) Mechanisms of apoptosis. *Biochem Mosc* 80:1393–1405. <https://doi.org/10.1134/S0006297915110012>
  29. Zhao H, Wang Y, Shao Y et al (2018) Oxidative stress-induced skeletal muscle injury involves in NF-κB/p53-activated immunosuppression and apoptosis response in copper (II) or/and arsenite-exposed chicken. *Chemosphere* 210:76–84. <https://doi.org/10.1016/j.chemosphere.2018.06.165>
  30. Jin YX, Pan XH, Cao LM et al (2013) Embryonic exposure to cis-bifenthrin enantioselectively induces the transcription of genes related to oxidative stress, apoptosis and immunotoxicity in zebrafish (*Danio rerio*). *Fish Shellfish Immun* 34:717–723. <https://doi.org/10.1016/j.fsi.2012.11.046>
  31. Fernández Freire P, Pérez Martín JM, Herrero O et al (2008) In vitro assessment of the cytotoxic and mutagenic potential of perfluorooctanoic acid. *Toxicol In Vitro* 22:1228–1233. <https://doi.org/10.1016/j.tiv.2008.04.004>
  32. Li Y, Pan L, Zeng X et al (2021) Ammonia exposure causes the imbalance of the gut-brain axis by altering gene networks associated with oxidative stress and immune function. *Ecotox Environ Safe* 224:112668. <https://doi.org/10.1016/j.ecoenv.2021.112668>
  33. Jin JL, Wang Y, Wu ZX et al (2017) Transcriptomic analysis of liver from grass carp (*Ctenopharyngodon idellus*) exposed to high environmental ammonia reveals the activation of antioxidant and apoptosis pathways. *Fish Shellfish Immun* 63:444–451. <https://doi.org/10.1016/j.fsi.2017.02.037>
  34. Abu-El-Zahab HSH, Hamza RZ, Montaser MM et al (2019) Antioxidant, antiapoptotic, antigenotoxic, and hepatic ameliorative effects of L-carnitine and selenium on cadmium-induced hepatotoxicity and alterations in liver cell structure in male mice. *Ecotox Environ Safe* 173:419–428. <https://doi.org/10.1016/j.ecoenv.2019.02.041>
  35. Schweizer U, Schomburg L, Savaskan NE (2004) The neurobiology of selenium: lessons from transgenic mice. *J Nutr* 134:707–710. <https://doi.org/10.1093/jn/134.4.707>
  36. Sadek KM, Lebda MA, Abouzed TK et al (2017) Neuro- and nephrotoxicity of subchronic cadmium chloride exposure and the potential chemoprotective effects of selenium. *Metab Brain Dis* 32:1659–1673. <https://doi.org/10.1007/s11011-017-0053-x>
  37. Zhang R, Liu Y, Xing L et al (2018) The protective role of selenium against cadmium-induced hepatotoxicity in laying hens: expression of Hsps and inflammation-related genes and modulation of elements homeostasis. *Ecotox Environ Safe* 159:205–212. <https://doi.org/10.1016/j.ecoenv.2018.05.016>
  38. Marettová E, Mareta M, Legáth J (2015) Toxic effects of cadmium on testis of birds and mammals: a review. *Anim Reprod Sci* 155:1–10. <https://doi.org/10.1016/j.anireprosci.2015.01.007>
  39. Cao C, Li X, Qin L et al (2018) High Selenium Yeast mitigates aluminum-induced cerebral inflammation by increasing oxidative stress and blocking NO production. *Biometals* 31:835–843. <https://doi.org/10.1007/s10534-018-0128-0>
  40. Phillips CJC, Pines MK, Latter M et al (2010) The physiological and behavioral responses of steers to gaseous ammonia in simulated long-distance transport by ship. *J Anim Sci* 88:3579–3589. <https://doi.org/10.2527/jas.2010-3089>

41. Wee NL, Tng YY, Cheng HT et al (2007) Ammonia toxicity and tolerance in the brain of the African sharp-toothed catfish *Clarias gariepinus*. *Aquat Toxicol* 82:204–213. <https://doi.org/10.1016/j.aquatox.2007.02.015>
42. Zhang Y, Guinnefollau L, Sullivan M et al (2018) Behaviour and physiology of sheep exposed to ammonia at a similar concentration to those experienced by sheep during export by sea. *Appl Anim Behav Sci* 205:34–43. <https://doi.org/10.1016/j.applanim.2018.05.017>
43. Boesveldt S (2017) Olfaction and eating behavior. In: Buettner A (ed) *Springer Handbook of Odor*. Springer, Germany, pp 109–110. [https://doi.org/10.1007/978-3-319-26932-0\\_44](https://doi.org/10.1007/978-3-319-26932-0_44)
44. Arnold G, Boer E, Boundy C (1980) The influence of odour and taste on the food preferences and food intake of sheep. *Aust J Agr Res* 31:571–587. <https://doi.org/10.1071/AR9800571>
45. Quarles C, Kling H (1974) Evaluation of ammonia and infectious bronchitis vaccination stress on broiler performance and carcass quality. *Poultry Sci* 53:1592–1596. <https://doi.org/10.3382/ps.0531592>
46. Sackett B, Fronting G, Deshazer J et al (1986) Effect of gaseous preslaughter environment on chicken broiler meat quality. *Poultry Sci* 65:511–519. <https://doi.org/10.3382/ps.0650511>
47. Wei F, Hu X, Sa R et al (2014) Antioxidant capacity and meat quality of broilers exposed to different ambient humidity and ammonia concentrations. *Genet Mol Res* 13:3117–3127. <https://doi.org/10.4238/2014.April.17.8>
48. Martins K, Applegate B, Hagedorn B et al (2015) Di(2-ethylhexyl) phthalate inhibits B cell proliferation and reduces the abundance of IgM-secreting cells in cultured immune tissues of the rainbow trout. *Fish & Shellfish Immun* 44:332–341. <https://doi.org/10.1016/j.fsi.2015.02.037>
49. Ghareeb K, Awad WA, Soodoi C et al (2013) Effects of feed contaminant deoxynivalenol on plasma cytokines and mRNA expression of immune genes in the intestine of broiler chickens. *PLoS One* 8:e71492. <https://doi.org/10.1371/journal.pone.0071492>
50. Balasubramanian S, Fan M, Messmer-Blust AF et al (2011) mGBP-2, an IFN- $\gamma$ -induced 67-kDa GTPase, inhibits TNF- $\alpha$  induction of Matrix Metalloproteinase-9 (MMP-9) transcription by inhibiting the activation of Rac and NF- $\kappa$ B. *Cytokine* 56:23. <https://doi.org/10.1016/j.cyto.2011.07.046>
51. Wang S, Li X, Wang W et al (2019) Application of transcriptome analysis: Oxidative stress, inflammation and microtubule activity disorder caused by ammonia exposure may be the primary factors of intestinal microvilli deficiency in chicken. *Sci Total Environ* 696:134035. <https://doi.org/10.1016/j.scitotenv.2019.134035>
52. Wang W, Chen MH, Jin X et al (2018) H<sub>2</sub>S induces Th1/Th2 imbalance with triggered NF- $\kappa$ B pathway to exacerbate LPS-induced chicken pneumonia response. *Chemosphere* 208:241–246. <https://doi.org/10.1016/j.chemosphere.2018.05.152>
53. Gao J, Zhu Y, Guo Z et al (2020) Transcriptomic analysis reveals different responses to ammonia stress and subsequent recovery between *Coilia nasus* larvae and juveniles. *Comp Biochem Phys C* 230:108710. <https://doi.org/10.1016/j.cbpc.2020.108710>
54. Ouyang WJ, O'Garra A (2019) IL-10 family cytokines IL-10 and IL-22: from basic science to clinical translation. *Immunity* 50:871–891. <https://doi.org/10.1016/j.immuni.2019.03.020>
55. Taylor-Robinson AW (1997) Counter-regulation of T helper 1 cell proliferation by nitric oxide and interleukin-2. *Biochem Biophys Res Commun* 233:14–19. <https://doi.org/10.1006/bbrc.1997.6386>
56. Xing H, Peng M, Li Z et al (2019) Ammonia inhalation-mediated mir-202-5p leads to cardiac autophagy through PTEN/AKT/mTOR pathway. *Chemosphere* 235:858–866. <https://doi.org/10.1016/j.chemosphere.2019.06.235>
57. Li Y, Zhang R, Li X et al (2021) Exposure to the environmental pollutant ammonia causes changes in gut microbiota and inflammatory markers in fattening pigs. *Ecotox Environ Safe* 208:111564. <https://doi.org/10.1016/j.ecoenv.2020.111564>
58. Anhe F, Nachbar R, Varin T et al (2019) Treatment with camu camu (*Myrciaria dubia*) prevents obesity by altering the gut microbiota and increasing energy expenditure in diet-induced obese mice. *Gut* 68:453–464. <https://doi.org/10.1136/gutjnl-2017-315565>
59. Shah SWA, Chen D, Zhang J et al (2020) The effect of ammonia exposure on energy metabolism and mitochondrial dynamic proteins in chicken thymus: Through oxidative stress, apoptosis, and autophagy. *Ecotox Environ Safe* 206:111413. <https://doi.org/10.1016/j.ecoenv.2020.111413>
60. Arnoult D, Rismanchi N, Grodet A et al (2005) Bax/Bak-dependent release of DDP/TIMM8a promotes Drp1-mediated mitochondrial fission and mitoptosis during programmed cell death. *Curr Biol* 15:2112–2118. <https://doi.org/10.1016/j.cub.2005.10.041>
61. Tilokani L, Nagashima S, Paupe V et al (2018) Mitochondrial dynamics: overview of molecular mechanisms. In: Garone C, Minczuk M (eds) *Mitochondrial Diseases*. pp 341–360. <https://doi.org/10.1042/EBC20170104>
62. Han Q, Zhang J, Sun Q et al (2020) Oxidative stress and mitochondrial dysfunction involved in ammonia-induced nephrocyte necroptosis in chickens. *Ecotox Environ Safe* 203:110974. <https://doi.org/10.1016/j.ecoenv.2020.110974>
63. Nelson WG, Kastan MB (1994) DNA strand breaks: the DNA template alterations that trigger p53-dependent DNA damage response pathways. *Mol Cell Biol* 14:1815–1823. <https://doi.org/10.1128/MCB.14.3.1815>
64. Fulda S, Gorman AM, Hori O et al (2010) Cellular stress responses: cell survival and cell death. *Int J Biochem Cell Biol* 2010:214074. <https://doi.org/10.1155/2010/214074>
65. Wang H, Wang A, Wang X et al (2022) AMPK/PPAR- $\gamma$ /NF- $\kappa$ B axis participates in ROS-mediated apoptosis and autophagy caused by cadmium in pig liver. *Environ Pollut* 294:118659. <https://doi.org/10.1016/j.envpol.2021.118659>
66. Jin X, Jia T, Liu R et al (2018) The antagonistic effect of selenium on cadmium-induced apoptosis via PPAR- $\gamma$ /PI3K/Akt pathway in chicken pancreas. *J Hazard Mater* 357:355–362. <https://doi.org/10.1016/j.jhazmat.2018.06.003>
67. Anne SL, Govek E-E, Ayrault O et al (2013) WNT3 inhibits cerebellar granule neuron progenitor proliferation and medulloblastoma formation via MAPK activation. *PLoS One* 8:e81769. <https://doi.org/10.1371/journal.pone.0081769>
68. Han Q, Liu H, Zhang R et al (2021) Selenomethionine protects against ammonia-induced apoptosis through inhibition of endoplasmic reticulum stress in pig kidneys. *Ecotox Environ Safe* 223:112596. <https://doi.org/10.1016/j.ecoenv.2021.112596>
69. Xu Z, Jin X, Pan T et al (2017) Antagonistic effects of selenium on cadmium-induced apoptosis by restoring the mitochondrial dynamic equilibrium and energy metabolism in chicken spleens. *Oncotarget* 8:52629–52641. <https://doi.org/10.18632/oncotarget.17539>
70. Cheng Z, Shu Y, Li X et al (2022) Evaluation of potential cardiotoxicity of ammonia: L-selenomethionine inhibits ammonia-induced cardiac autophagy by activating the PI3K/AKT/mTOR signaling pathway. *Ecotox Environ Safe* 233:113304. <https://doi.org/10.1016/j.ecoenv.2022.113304>

**Publisher's Note** Springer Nature remains neutral with regard to jurisdictional claims in published maps and institutional affiliations.

Springer Nature or its licensor holds exclusive rights to this article under a publishing agreement with the author(s) or other rightsholder(s); author self-archiving of the accepted manuscript version of this article is solely governed by the terms of such publishing agreement and applicable law.